Syndromic deafness mutations at Asn 14 differentially alter the open stability of Cx26 hemichannels

Helmuth A. Sanchez,[1] Nefeli Slavi,[2] Miduturu Srinivas,[2] and Vytas K. Verselis[1]

[1]Dominick P. Purpura Department of Neuroscience, Albert Einstein College of Medicine, Bronx, NY 10461
[2]Department of Biological Sciences, SUNY College of Optometry, New York, NY 10036

Connexin 26 (Cx26) is a transmembrane protein that forms hexameric hemichannels that can function when unopposed or dock to form intercellular gap junction channels. Aberrantly functioning unopposed hemichannels are a common feature of syndromic deafness associated with mutations in Cx26. In this study, we examine two different mutations at the same position in the N-terminal domain of Cx26, N14K and N14Y, which have been reported to produce different phenotypes in patients. We find that both N14K and N14Y, when expressed alone or together with wild-type (WT) Cx26, result in functional hemichannels with widely disparate functional properties. N14K currents are robust, whereas N14Y currents are small. The two mutants also exhibit opposite shifts in voltage-dependent loop gating, such that activation of N14K and N14Y is shifted in the hyperpolarizing and depolarizing directions, respectively. Deactivation kinetics suggests that N14K stabilizes and N14Y destabilizes the open state. Single N14K hemichannel recordings in low extracellular Ca^{2+} show no evidence of stable closing transitions associated with loop gating, and N14K hemichannels are insensitive to pH. Together, these properties cause N14K hemichannels to be particularly refractory to closing. Although we find that the unitary conductance of N14K is indistinguishable from WT Cx26, mutagenesis and substituted cysteine accessibility studies suggest that the N14 residue is exposed to the pore and that the differential properties of N14K and N14Y hemichannels likely result from altered electrostatic interactions between the N terminus and the cytoplasmic extension of TM2 in the adjacent subunit. The combined effects that we observe on loop gating and pH regulation may explain the unusual buccal cutaneous manifestations in patients carrying the N14K mutation. Our work also provides new considerations regarding the underlying molecular mechanism of loop gating, which controls hemichannel opening in the plasma membrane.

INTRODUCTION

Keratitis ichthyosis deafness (KID) syndrome is one of several syndromes associated with mutations in *GJB2* encoding the connexin 26 (Cx26) gap junction (GJ) channel protein. KID syndrome patients typically exhibit profound prelingual sensorineural hearing loss, widespread erythrokeratoderma, vascularizing keratitis that leads to visual impairment, dystrophic nails, and predisposition to squamous cell carcinomas (Coggshall et al., 2013). Classically, connexins are viewed as substrates of intercellular GJ channels, which are formed by the docking of two so-called hemichannels, one each contributed by two apposed cells. However, the undocked hemichannels can function as well, contributing to signaling across the plasma membrane. A common property among KID syndrome mutants, as well as other Cx26 syndromic deafness mutants, is aberrantly functioning hemichannels, suggesting that gain of function mediated by Cx26 hemichannels is a principal contributor to cellular pathology (Lee and White, 2009; Xu and Nicholson, 2013; Sanchez and Verselis, 2014).

Thus far, mutations at eight amino acid positions have been identified in patients with KID syndrome. Interestingly, these mutations cluster predominantly in two domains, the first extracellular loop domain (E1), linking the first two of four transmembrane domains, and the cytoplasmic N-terminal (NT) domain. These regions have been shown to contribute to the aqueous pore and to contain elements critical for voltage-dependent gating (Verselis et al., 1994, 2009; Zhou et al., 1997; Pfahnl and Dahl, 1998; Oh et al., 1999; Purnick et al., 2000b; Kronengold et al., 2003; Maeda et al., 2009; Tang et al., 2009; Verselis, 2009; Sanchez et al., 2010). Three mutants clustered in the E1 domain, A40V, G45E, and D50N, have been examined in some detail and show a range of aberrant hemichannel properties including shifted voltage-dependent gating, altered permeability, and impaired inhibition by extracellular Ca^{2+} and pH (Gerido et al., 2007; Lee et al., 2009; Sanchez et al., 2010, 2013, 2014). Mutants in the NT domain have been less well characterized, but impaired inhibition by Ca^{2+} has been described for N14K, G12R, and G11E mu-

Correspondence to Vytas K. Verselis: vytas.verselis@einstein.yu.edu

Abbreviations used in this paper: GJ, gap junction; IPS, internal patch solution; KID, keratitis ichthyosis deafness; MTS, methanethiosulfonate; NT, N-terminal; WT, wild type.

© 2016 Sanchez et al. This article is distributed under the terms of an Attribution–Noncommercial–Share Alike–No Mirror Sites license for the first six months after the publication date (see http://www.rupress.org/terms). After six months it is available under a Creative Commons License (Attribution–Noncommercial–Share Alike 3.0 Unported license, as described at http://creativecommons.org/licenses/by-nc-sa/3.0/).

The Rockefeller University Press $30.00
J. Gen. Physiol. 2016 Vol. 148 No. 1 25–42
www.jgp.org/cgi/doi/10.1085/jgp.201611585

The Journal of General Physiology

Downloaded from http://rupress.org/jgp/article-pdf/148/1/25/1795860/jgp_201611585.pdf by guest on 04 December 2025

tant hemichannels (Lee et al., 2009; Terrinoni et al., 2010). At the N14 position, two different mutations have been identified, N14K and N14Y (van Steensel et al., 2004; Arita et al., 2006). The cutaneous manifestations associated with these mutations differ. Patients carrying the N14Y mutation show considerable overlap with KID syndrome (Arita et al., 2006; de Zwart-Storm et al., 2011), whereas patients carrying the N14K mutation lack keratitis and exhibit uncharacteristic mucocutaneous manifestations such as lip fissuring, gingival swelling, and hyperemia with erosions of the tongue and buccal mucosa (van Steensel et al., 2004; Lazic et al., 2008). Thus, the chemical nature of the amino acid substitution at N14 appears to have a significant impact on disease manifestation.

Here, we examined the properties of N14K and N14Y hemichannels expressed in *Xenopus laevis* oocytes to assess whether there are notable differences that can contribute to the distinctive phenotypes exhibited in patients. Indeed, the properties of the two mutant hemichannels differed substantially in several ways, most notably in the magnitude of membrane current produced and in the direction activation was shifted for the loop gating mechanism that governs their opening in the plasma membrane. Also, sensitivity to pH was essentially abolished in N14K hemichannels. Cysteine substitution and subsequent modification with thiol-modifying methanethiosulfonate (MTS) reagents indicate that N14 is accessible through the pore. Although positive charge substitution at this position did not impact unitary conductance, our data suggest it could produce an electrostatic effect with the cytoplasmic extension of the TM2 domain that leads to stabilization of the open conformation of the loop gating mechanism and the differential gating phenotype between N14K and N14Y hemichannels. Altered gating coupled with a loss of sensitivity to pH for N14K could be responsible for the uncharacteristic mucocutaneous manifestations exhibited by patients.

MATERIALS AND METHODS

Construction of Cx26 mutants

Human wild-type (WT) Cx26 was cloned into the BamHI restriction site of the pCS2$^+$ expression vector for functional studies in *Xenopus* oocytes. All site-directed mutations were constructed using the QuikChange mutagenesis kit (Agilent Technologies) in accordance with the manufacturer's protocol using the WT connexin expression constructs as templates. All constructs were verified by sequencing.

Exogenous expression of connexins

For expression of connexins in *Xenopus* oocytes, RNA was synthesized, and oocytes were prepared and injected as previously described (Trexler et al., 2000; Sanchez et al., 2010). Injected oocytes were maintained at 16–18°C in a modified ND96 solution (MND96) containing (in mM) 100 NaCl, 2 KCl, 1 $MgCl_2$, 1.8 $CaCl_2$, 10 glucose, 10 HEPES, and 5 pyruvate, with the pH adjusted to 7.6.

Reagents

The MTS reagents 2-aminoethylmethanethiosulfonate (MTSEA), 2-trimethylammonioethylmethane thiosulfonate (MTSET), and 2-sulfonatoethylmethanethiosulfonate (MTSES) were purchased from Anatrace. 2-(6-biotinoylamino)hexanoyl-aminoethylmethanethiosulfonate (MTSEA biotin), 2-((6-((biotinoyl)amino)hexanoyl)amino) ethylmethanethiosulfonate (MTSEA biotin-X), and 2-((6-((6-((biotinoyl)amino)hexanoyl)amino)hexanoyl) amino)ethylmethanethiosulfonate (MTSEA biotin-XX) were purchased from Biotium. Aliquots of dry powder were prepared and stored in microcentrifuge tubes at −20°C. Before each experiment, aliquots of MTSEA, MTSET, and MTSES were dissolved in distilled water and chilled on ice to stock concentrations of 100–200 mM. MTSEA biotin, MTSEA biotin-X, and MTSEA biotin-XX were dissolved in DMSO. Dilutions were made into appropriate perfusion solutions just before application to a final concentration of 0.2 mM for MTSEA, MTSET, MTS EA biotin, MTSEA biotin-X, and MTSEA biotin-XX and 2 mM for MTSES. The activity of MTS reagents was periodically checked using the TNB (2-nitro-5-thiobenzoate) assay (Karlin and Akabas, 1998).

Macroscopic electrophysiological recording

Macroscopic Cx26 hemichannel currents were recorded as previously described (Sanchez et al., 2010, 2013, 2014). In brief, oocytes were placed in a polycarbonate RC-1Z recording chamber (Warner Instruments) with inflow and outflow compartments. The outflow compartment contained agar bridges connected to a VG-2A virtual ground bath clamp (Molecular Devices). All recordings were obtained with a two-electrode voltage clamp (GeneClamp 500; Molecular Devices). Both current-passing and voltage-recording pipettes contained 1 M KCl. During recording, oocytes were perfused with simple salt solutions that contained (in mM) 100 NaCl, 1 $MgCl_2$, and 10 HEPES, to which Ca^{2+} and/or NaOH was adjusted to achieve desired Ca^{2+} and pH values.

Single hemichannel recording

For patch clamp recordings of single hemichannel currents, *Xenopus* oocytes were manually devitellinized in a hypertonic solution consisting of (in mM) 220 Na-aspartate, 10 KCl, 2 $MgCl_2$, and 10 HEPES and then placed in MND96 for recovery. Oocytes were then individually moved to a recording chamber (RC-28; Warner Instruments) containing an internal patch solution (IPS), which consisted of (in mM) 140 KCl, 1 $MgCl_2$, 5

Downloaded from http://rupress.org/jgp/article-pdf/148/1/25/1795860/jgp_201611585.pdf by guest on 04 December 2025

HEPES, 1 $CaCl_2$, and 3 EGTA, and pH was adjusted to 8.0 with KOH. The bath compartment was connected via a 30 M agar bridge to a ground compartment containing the same IPS solution. After excision of patches, hemichannels were exposed to symmetric solutions, and any instrumentation offsets were manually corrected in the absence of an applied voltage. Single hemichannel I-V curves were obtained by applying 8-s voltage ramps from −70 to 70 mV. Currents were leak subtracted by measuring leak conductance of a given patch from full closing transitions or loss of channel activity and extrapolating linearly over the entire voltage range. Currents were typically filtered at 1 kHz, and data were acquired at 5 kHz.

Acquisition of electrophysiological data

In electrophysiological experiments using oocytes, data were acquired with AT-MIO-16X D/A boards from National Instruments using custom acquisition and analysis software (written by E.B. Trexler, Gotham Scientific, Hasbrouck Heights, NJ).

Online supplemental material

Fig. S1 demonstrates that reactivity of N14C to MTS reagents increases with hemichannel opening induced by depolarization or co-injection with WT Cx26. Fig. S2 illustrates that the kinetics of the responses of N14K hemichannels to extracellular Ca^{2+} are slowed. Online supplemental material is available at http://www.jgp.org/cgi/content/full/jgp.201611585/DC1.

RESULTS

N14K and N14Y hemichannels exhibit substantial differences in functional efficiency and gating

N14K and N14Y both produced functional hemichannels when expressed in *Xenopus* oocytes (Fig. 1). Mean currents recorded in low (0.2 mM) extracellular Ca^{2+}, which promotes hemichannel opening, were robust for N14K but were small for N14Y injected with the same concentration of mRNA. Similar results were obtained when N14K and N14Y mutants were coexpressed with WT Cx26 in 1:1 ratios, indicating that N14Y exerts a dominant-negative effect on WT Cx26 hemichannel function. In 2.0 mM Ca^{2+}, currents for N14K, like WT Cx26, were substantially inhibited, particularly at hyperpolarized potentials. Currents remained small and barely detectible for N14Y.

Voltage-dependent gating properties of N14K and N14Y hemichannels also differed. Fig. 2 shows G-V relationships and families of currents for WT Cx26, N14K, and N14Y hemichannels at two extracellular Ca^{2+} concentrations, 0.2 mM and 2.0 mM. Cx26 hemichannels, like all connexin hemichannels, close on hyperpolarization via the loop (or slow) gating mechanism that is sensitive to extracellular Ca^{2+} (Fig. 2 A). Activation shifts

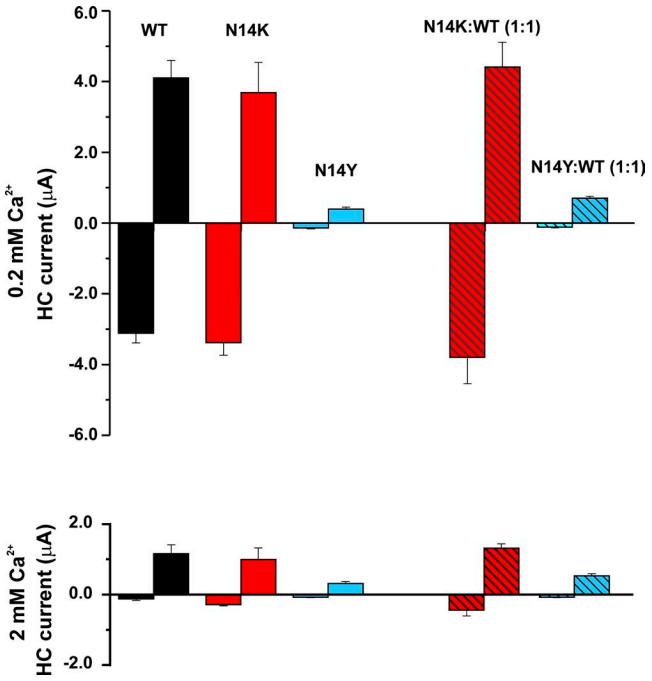

Figure 1. **Functional expression of N14K and N14Y hemichannels.** Bar graphs show mean values of hemichannel (HC) currents measured in *Xenopus* oocytes at a holding potential of −40 mV and at the end of a 10-s voltage step to 40 mV. Measurements were obtained in 100 mM NaCl containing 0.2 mM Ca^{2+} (top) or 2.0 mM Ca^{2+} (bottom). N14K produced robust currents comparable with WT Cx26 in 0.2 mM Ca^{2+}. Currents were substantially inhibited in 2 mM Ca^{2+}. N14Y produced very small currents at both Ca^{2+} concentrations, particularly when measured at −40 mV, which were barely detectable above baseline. N14K and N14Y, each co-injected with WT Cx26 in a 1:1 ratio, showed similar differential levels of expressed currents. All oocytes were injected with the same concentration of total RNA. Measurements were obtained between 24 and 48 h, after injection. Each bar represents the mean ± SEM obtained at −40 mV and 40 mV. In 0.2 mM Ca^{2+}: WT Cx26, n = 7; N14K, n = 13; N14Y, n = 11; N14K:WT, n = 8; N14Y:WT, n = 10. In 2 mM Ca^{2+}: WT Cx26, n = 12; N14K, n = 9; N14Y, n = 19; N14K:WT, n = 6; N14Y:WT, n = 19.

positive with Ca^{2+}, effectively reducing hemichannel opening at negative membrane potentials. N14K hemichannels retained sensitivity to extracellular Ca^{2+} but differed from WT Cx26 hemichannels in showing little or no evidence of voltage-dependent reductions in conductance upon hyperpolarization in lower Ca^{2+} (0.2 mM) conditions (Fig. 2 B). Conversely, N14Y hemichannels appeared to be less sensitive to Ca^{2+} but notably exhibited strong voltage dependence in 2.0 mM and 0.2 mM Ca^{2+} (Fig. 2 C). In 0.2 mM Ca^{2+}, N14Y exhibited a positive shift in activation compared with WT Cx26, which can further contribute to low hemichannel currents for this mutant at hyperpolarized potentials.

Superimposition of normalized G-V curves for WT Cx26, N14K, and N14Y in 0.2 mM extracellular Ca^{2+} illustrates the opposite shifts in activation for N14K and

Downloaded from http://rupress.org/jgp/article-pdf/148/1/25/1795860/jgp_201611585.pdf by guest on 04 December 2025

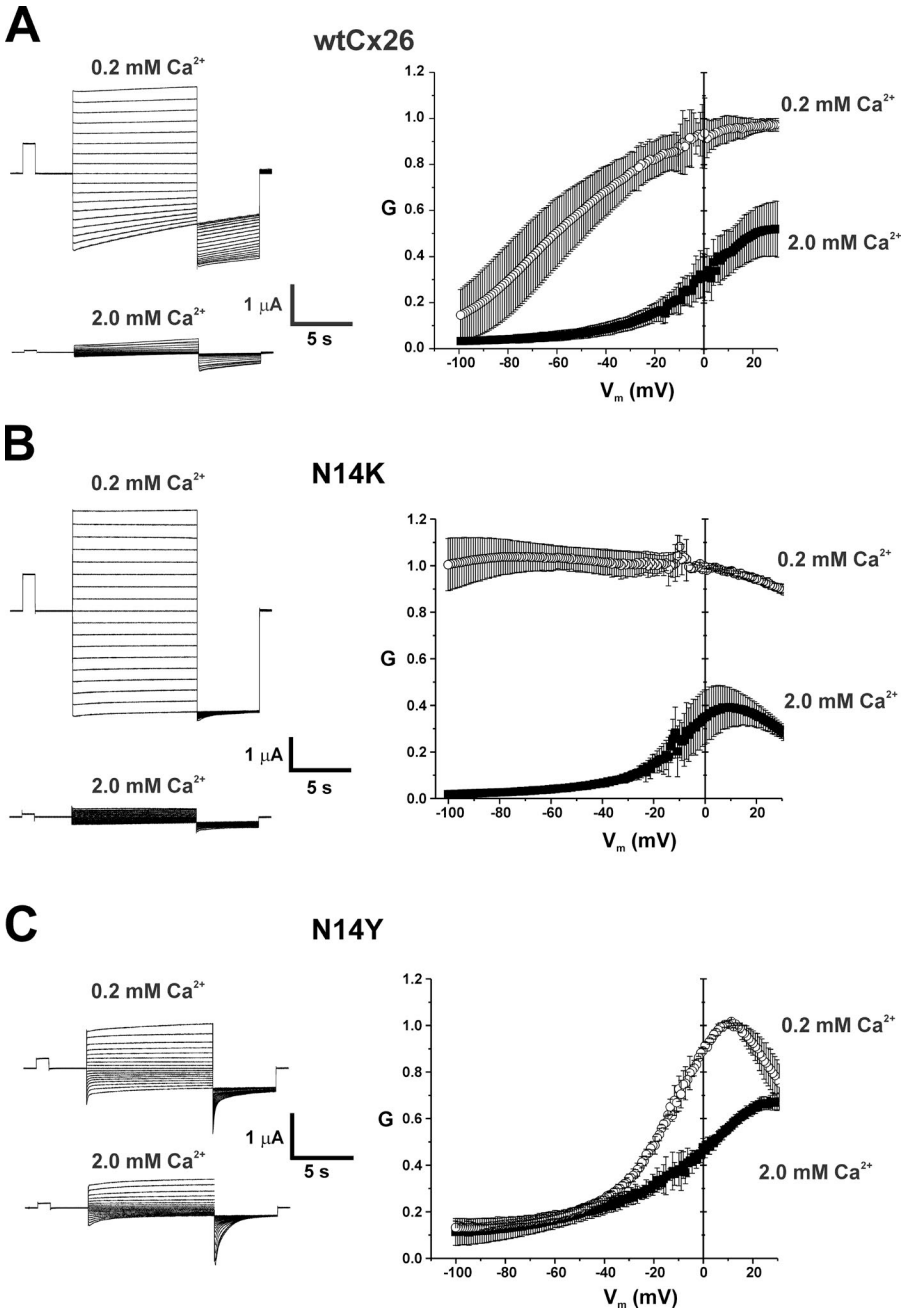

Figure 2. **N14K and N14Y mutations produce differential shifts in voltage-dependent loop gating.** Shown are representative families of currents from WT Cx26, N14K, and N14Y hemichannels at two different external Ca^{2+} concentrations, 0.2 mM and 2 mM. Currents were elicited using a voltage step protocol consisting of 10-s steps, from 60 to −110 mV in intervals of 10 mV, followed by a 5-s step to −110 mV; oocytes were voltage clamped to −20 mV between steps. Accompanying these currents are normalized G-V relationships at 0.2 mM and 2 mM Ca^{2+}. Data were obtained by applying slow (600 s) voltage ramps from 40 to −100 mV from a holding potential of −20 mV. Ramps were applied to each oocyte in 0.2 and 2.0 mM Ca^{2+}, and the calculated conductances were normalized to the maximum value measured in 0.2 mM Ca^{2+}. N14K continued to show robust inhibition by Ca^{2+}, but conductance remained essentially constant with hyperpolarization in 0.2 mM Ca^{2+}. The G-V relationship for N14Y in 0.2 mM Ca^{2+} was shifted substantially positive along the voltage axis compared with WT Cx26, and Ca^{2+} appears to have a relatively modest effect. Each symbol represents the mean value. Error bars are ±SEM. WT Cx26, n = 5; N14K, n = 5; N14Y, n = 4.

N14Y when expressed alone (Fig. 3 A) or together with WT Cx26 in 1:1 ratios (Fig. 3 B).

Examination of the tail currents after activation revealed considerably faster kinetics of closure for N14Y compared with WT Cx26 (Fig. 3 C). Although not strictly quantified, the approximate time for the current to decline by 70% was ∼0.5 s for N14Y at −100 mV, which is ∼10-fold faster than for WT Cx26. N14K currents essentially remained constant when stepped to −100 mV. These data suggest that the N14Y substitution produces a destabilization of the open state of the loop gating mechanism, whereas the N14K substitution has the opposite effect, producing a stabilization of the open state.

Single N14K hemichannels: Effects on voltage-dependent gating

In cell-attached and excised inside-out or outside-out patch configurations, we found that the N14K substitution did not affect unitary conductance (Fig. 4 A). Voltage ramps applied to patches containing single N14K hemichannels exhibited a similar slope conductance to WT Cx26 (336 ± 18 for N14K vs. 340 ± 9 for WT) and slight outward rectification in symmetric KCl solutions. Levels of N14Y currents were low, and we were unable to record unitary events.

Next, we examined gating at the level of single hemichannels (Fig. 4 B). For WT Cx26 in the presence of EGTA to chelate Ca^{2+} to submicromolar levels, loop gat-

Downloaded from http://rupress.org/jgp/article-pdf/148/1/25/1795860/jgp_201611585.pdf by guest on 04 December 2025

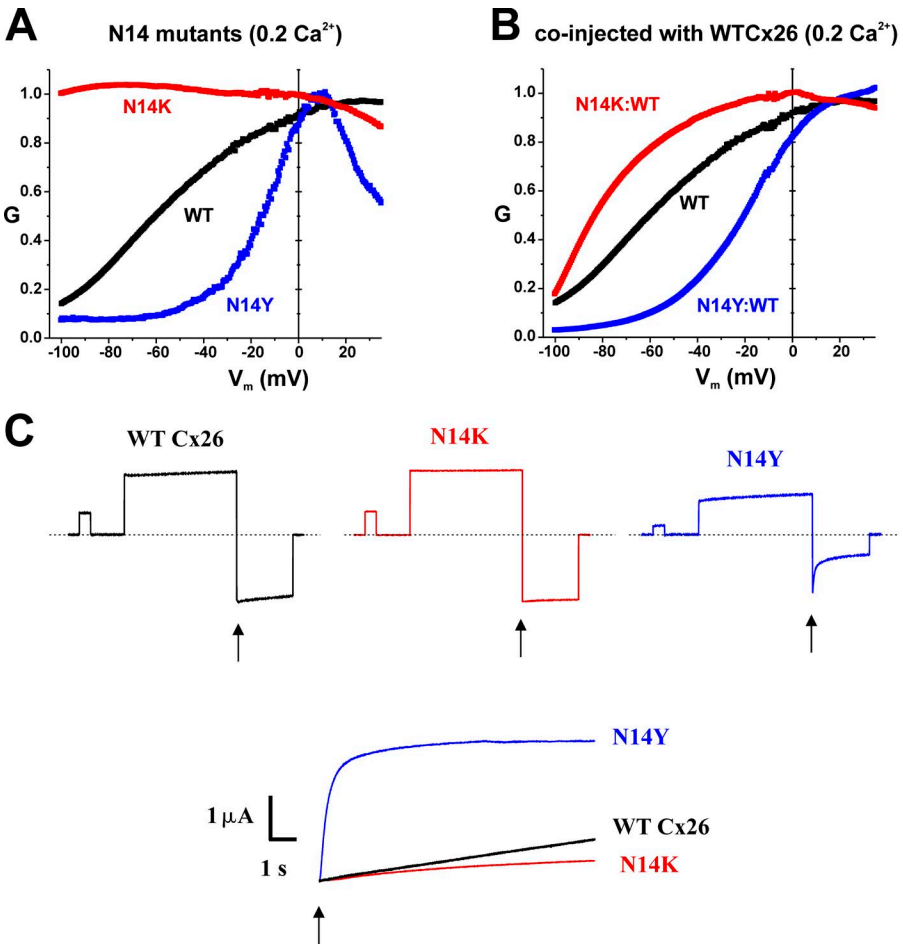

Figure 3. **N14K and N14Y likely affect the stabilization of the open state for the loop gating mechanism.** (A and B) Superimposition of the normalized G-V curves in 0.2 mM Ca^{2+} for WT and for the two mutants N14K and N14Y, expressed alone (A) and together with WT Cx26 in 1:1 ratios (B), shows the opposite shifts in activation caused by the two mutants. Data in A is the same as in Fig. 2. Error bars were omitted for clarity. N14K:WT, n = 5; N14Y:WT, n = 6; WT, n = 5. (C) Examples of deactivation kinetics for WT Cx26, N14K, and N14Y hemichannels. Cells were stepped to 40 mV for 16 s to activate hemichannels and then stepped to −100 mV (at arrows) to examine deactivation. Currents were superimposed at their peaks. N14Y currents deactivated rapidly compared with WT Cx26. N14K did not show appreciable deactivation.

ing closures can be elicited with strong hyperpolarization. However, Cx26 hemichannels exhibited frequent loop gating even at voltages that did not produce time-dependent reductions in macroscopic conductance. Thus, in addition to voltage-dependent loop gating, Cx26 hemichannels exhibit voltage-independent or constitutive loop gating, transiting often between stable open and closed states. This property was evident in other KID mutants as well, shown here in Fig. 4 B for A40V and G45E. In striking contrast, stable loop gating transitions to the closed state were essentially lacking in N14K hemichannels, even at large negative potentials. The N14K hemichannel continued to show frequent, brief flickers from the open state that were poorly resolved and did not settle into a stable conductance level. It is unknown whether these flickers are incomplete attempts at closure of the loop gate or some other conformational events.

Loop gating is one of two voltage-sensitive gating mechanisms in connexin hemichannels. The other mechanism, termed V_j or fast gating (Bukauskas and Verselis, 2004), closes hemichannels to a residual subconducting state and for Cx26 has the opposite gating polarity to loop gating, with closure to the subconducting state occurring at positive membrane voltages. To assess whether the N14K mutation abolished V_j gating as well, we recorded from cell-attached patches containing N14K hemichannels over a range of membrane potentials. A representative recording from a patch shows no loop gating at negative voltages but typical V_j gating at positive voltages characterized by gating to subconducting states (Fig. 5 A). Because large positive voltage steps beyond 40 mV can elicit endogenous currents in macroscopic recordings, we examined V_j gating further in patch recordings that were devoid of contaminating channels. G-V curves derived from ensemble averages of ramps applied between −40 and 70 mV show reductions in conductance at positive voltages for both WT Cx26 and N14K (Fig. 5 B). Although these are not steady-state recordings, the G-V curve for N14K was very similar to that for WT Cx26.

Sensitivity to pH is severely impaired in N14K hemichannels

pH robustly regulates WT Cx26 hemichannels in a physiological range with an apparent pK near 7.3 (Ripps et al., 2004; Sanchez et al., 2014). However, N14K hemichannels showed no sensitivity in this pH range. Fig. 6 A shows the macroscopic conductance ratios relative to pH 8.0 with cells held at −40 mV for two test pH values,

Downloaded from http://rupress.org/jgp/article-pdf/148/1/25/1795860/jgp_201611585.pdf by guest on 04 December 2025

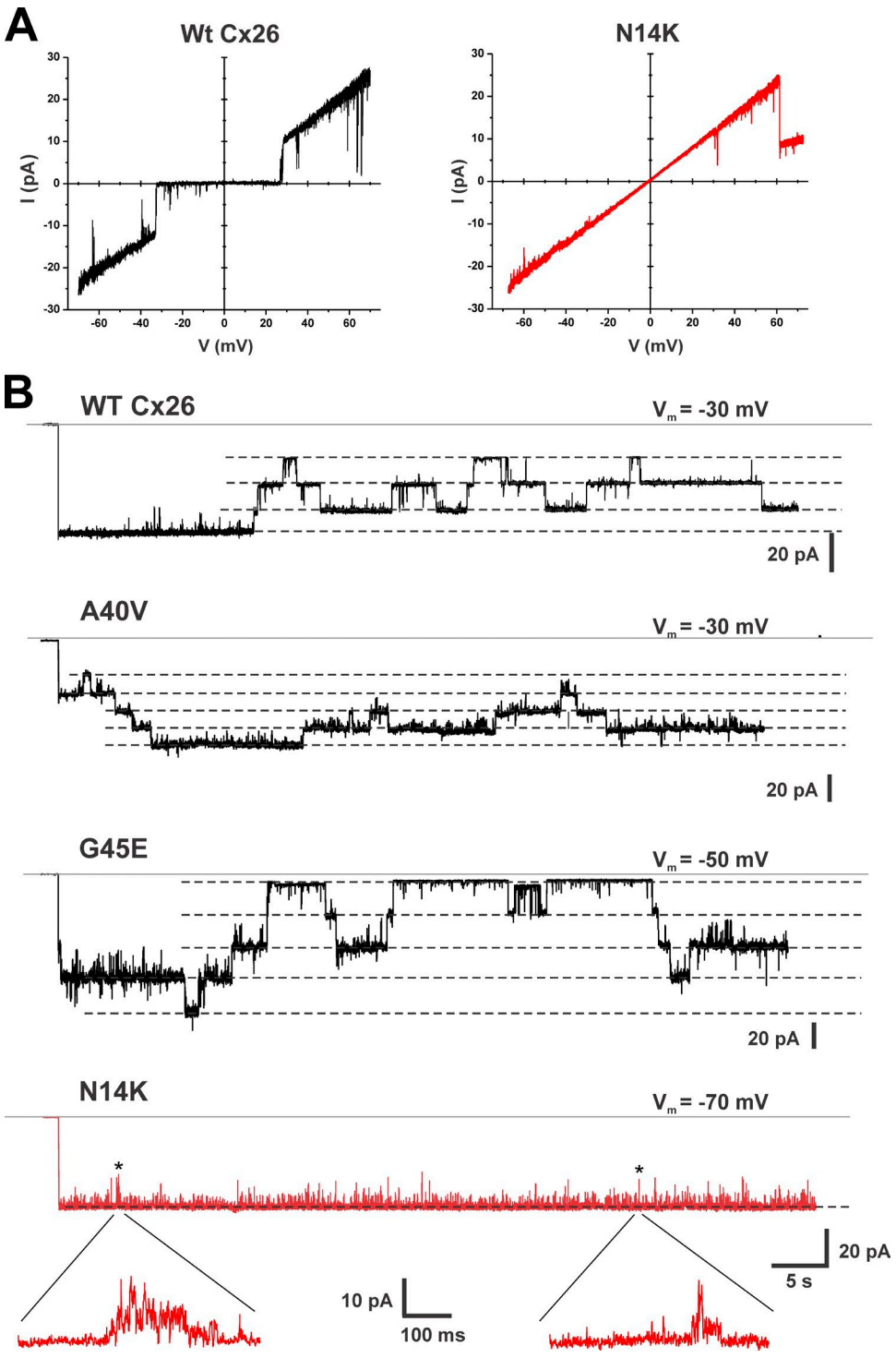

Figure 4. **Single N14K hemichannel recordings show a stably open configuration.** (A) Representative examples of patch clamp recordings from inside-out patches containing single WT Cx26 and N14K hemichannels. Currents shown were obtained in response to 8-s voltage ramps applied between 70 and −70 mV and leak subtracted (see Materials and methods). N14K is indistinguishable from WT Cx26 in terms of slope conductance (measured at 0 mV) and slight outward rectification. Bath and pipette solutions consisted of IPS (see Materials and methods). (B) Examples of patch clamp recordings of WT Cx26 hemichannels and three KID mutants, A40V, G45E, and N14K. Patches contained two or more active hemichannels. At the beginning of each trace, the membrane potential was stepped from 0 mV to the value indicated. WT Cx26, A40V, and G45E all showed active loop gating events throughout. N14K (red trace) showed a clear difference from the other hemichannels, essentially remaining open with no evidence of stable loop gating closures, consistent with stabilization of the open configuration for this gating mechanism. Examples of expanded views of the brief flickers (at asterisks) show them to be poorly resolved, noisy fluctuations in current that do not reach a steady level. Solid lines are the currents at 0 mV (designated $I = 0$). Dashed lines indicate open hemichannel current levels. The records were not leak subtracted. All currents were filtered at 1 kHz, and data were acquired at 5 kHz.

Downloaded from http://rupress.org/jgp/article-pdf/148/1/25/1795860/jgp_201611585.pdf by guest on 04 December 2025

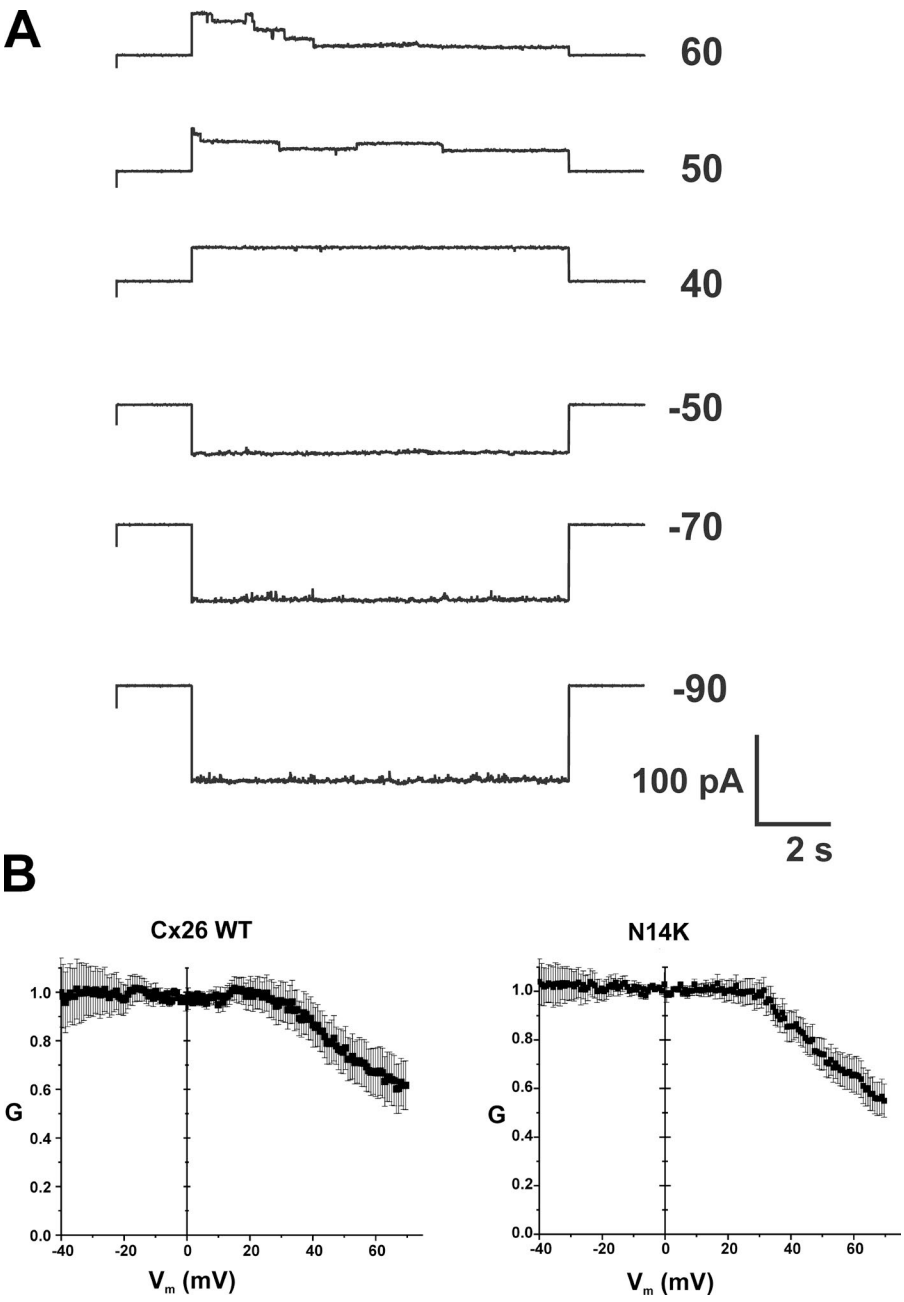

Figure 5. **The N14K mutation selectively affects the loop gating mechanism.** (A) Representative cell-attached patch recording containing several N14K hemichannels. Pipettes contained IPS so that Ca^{2+} was buffered to submicomolar levels. The patch was stepped to voltages ranging from −90 to 60 mV for 10 s. No gating was evident with hyperpolarizing steps, but gating to subconductance states was evident on depolarizing steps characteristic of the V_j or fast gating mechanism. (B) G-V relationships at positive voltages were constructed from voltage ramps applied to patches containing one or two active hemichannels. For WT Cx26 and N14K, currents were each averaged from 50 to 60 ramps taken from eight different oocytes. The G-V curves at positive membrane voltages appear similar for WT and N14K. Error bars are ±SEM. All currents were filtered at 1 kHz, and data were acquired at 5 kHz.

7.1 and 6.5; conductance plateaus to a maximum at pH 8.0 (Sanchez et al., 2014). Data are shown for WT, N14K, and N14K co-injected with WT Cx26 in ratios of 1:1 and 1:4. For WT Cx26, conductance declined by ∼70% when pH was reduced to 7.1, whereas N14K showed no measureable decline at pH 7.1. Oocytes co-injected with N14K and WT Cx26 also exhibited no measureable decline for a 1:1 ratio and a modest decline for a 1:4 ratio (N14K/WT). Exposure to a lower pH of 6.5 also had little effect on N14K currents but showed progressive reductions of ∼15% and ∼50% for N14/WT ratios of 1:1 and 1:4, respectively. For WT Cx26, currents declined by ∼90% at pH 6.5. Thus, N14K hemichannels are rendered insensitive to pH in a physiological range and the mutant acts in a dominant manner when coexpressed with WT Cx26 to hamper inhibition by pH. The currents for N14Y were too small to assess pH sensitivity in the same way as we did for N14K. Thus, we examined pH responses at a positive potential of 40 mV. Data are shown for WT, N14K, N14Y, and both mutants co-injected with WT Cx26 in a 1:1 ratio (Fig. 6 B). Sensitivity to pH of WT Cx26 was somewhat reduced at 40 mV. N14K remained insensitive to pH. N14Y appeared to have an intermediate sensitivity to pH, particularly evident at pH 6.5, indicating some impairment of inhibition by pH.

Downloaded from http://rupress.org/jgp/article-pdf/148/1/25/1795860/jgp_201611585.pdf by guest on 04 December 2025

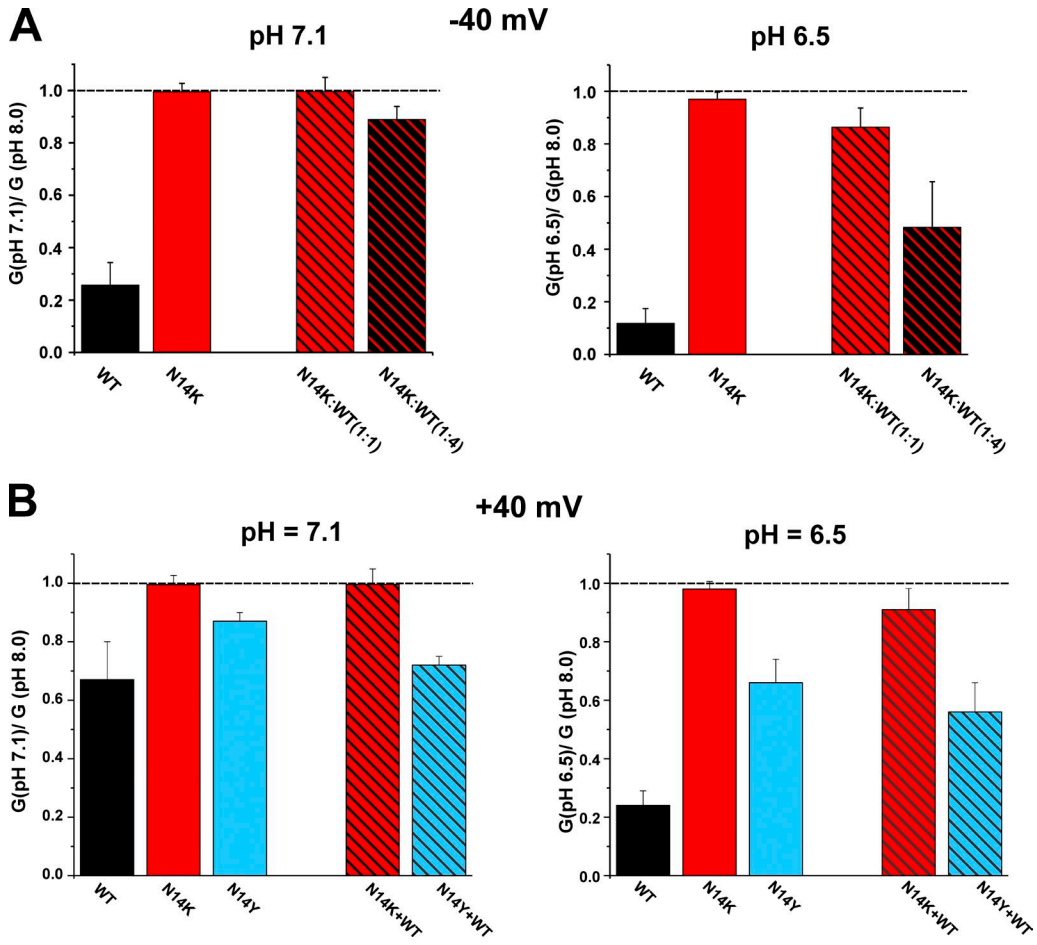

Figure 6. **The N14K mutation is insensitive to pH.** The bar graphs show ratios of macroscopic conductances relative to pH 8.0 in solutions adjusted to pH 7.1 and 6.5. (A) Conductances were calculated from oocytes held at −40 mV. Data are shown for WT Cx26, N14K, and N14K co-injected with WT Cx26 (N14K:WT) in ratios of 1:1 and 1:4. N14K hemichannels were insensitive to either pH 7.1 or 6.5. Hemichannel currents recorded from cells co-injected in a 1:1 ratio also were largely refractory to inhibition by pH, whereas those co-injected in a 1:4 ratio showed weakened but progressive reductions with pH 7.1 and 6.5. WT Cx26, $n = 6$; N14K, $n = 4$; N14K:WT (1:1), $n = 9$; N14K:WT (1:4), $n = 4$. (B) N14Y currents are small at negative membrane voltages, and so the effects of pH were assessed for this mutant at 40 mV. Data are shown for WT Cx26, N14K, N14Y, and each mutant co-injected with WT Cx26 in a 1:1 ratio (N14K + WT and N14Y + WT). N14K hemichannels remained insensitive to pH. N14Y showed reduced sensitivity that was intermediate between WT and N14K. WT Cx26, $n = 4$; N14K, $n = 4$; N14Y, $n = 5$; N14K + WT (1:1), $n = 4$; N14Y:WT (1:4), $n = 5$. Each bar represents the mean ratio ± SEM.

N14 and the hemichannel pore

The eight residues identified thus far as mutated in KID syndrome are depicted in the crystal structure of Cx26 (Fig. 7). N14 is positioned at the cytoplasmic vestibule, and, if exposed to the aqueous pore as suggested by this structure, the N14K mutation would introduce a ring of six positive charges in the path of permeating ions and molecules. Yet, as we showed in Fig. 4 A, recordings of single hemichannels showed no change in the unitary conductance produced by the N14K mutation. Thus, to further probe whether N14 is indeed exposed to the pore, we made a cysteine substitution and examined accessibility to the thiol-modifying MTS reagents. However, oocytes injected with the N14C mutation often showed currents barely detectible above baseline. Bath application of the reducing and metal-chelating agent dithiothreitol had no effect, indicating impaired hemichannel function was not caused by disulfide or metal bridge formation (unpublished data).

Next, we applied MTS reagents to the bath. Application of MTSET to oocytes held at −40 mV had little to no effect on the current, whereas application of MTSEA led to a rapid and robust induction of current to levels comparable with those observed with WT Cx26 or N14K hemichannels (Fig. 8 A). The strong induction of current with MTSEA suggests that this reagent modified the N14C side chain and restored hemichannel function. The effectiveness of MTSEA, but not MTSET, can be explained by the charge characteristics of these reagents. MTSET carries a permanent positive charge, rendering it membrane impermeant. With N14 located toward the cytoplasmic end of the hemichannel,

Downloaded from http://rupress.org/jgp/article-pdf/148/1/25/1795860/jgp_201611585.pdf by guest on 04 December 2025

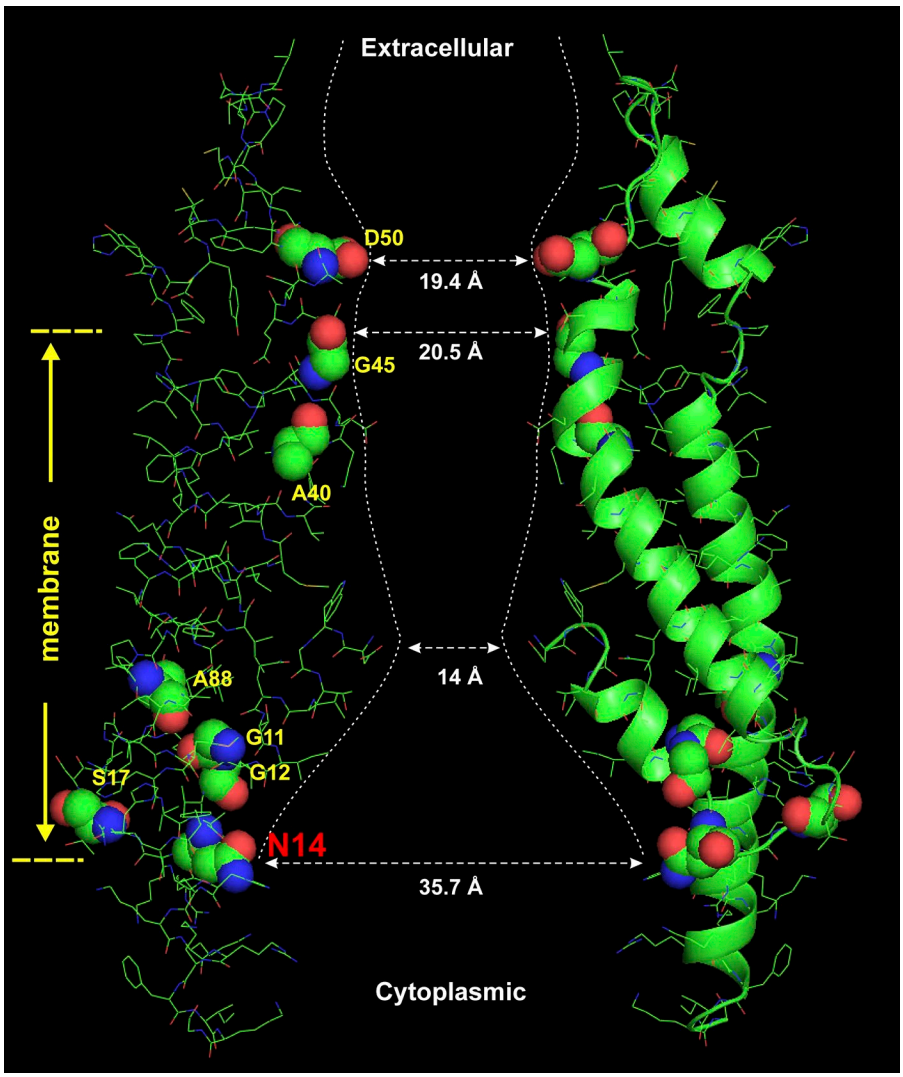

Figure 7. **Positions of N14 and other KID mutants in the Cx26 structure.** Representation of two of six subunits (in green) around a central aqueous pore from the atomic structure of Cx26 (Protein Data Bank accession no. 2ZW3; Maeda et al., 2009). The structure is displayed using the PyMOL Molecular Graphics System (version 1.8; Schrödinger, LLC). For clarity, the Cx26 sequence shown is truncated at residue G109 near the border of the cytoplasmic TM2 extension and the cytoplasmic loop. KID mutant residues are shown as spherical renditions. The gross shape of the pore is illustrated by the dashed lines, with approximate dimensions of the pore diameter at various positions. The approximate membrane boundary is indicated. In this structure, N14 is situated in the wide cytoplasmic vestibule of the hemichannel.

bath-applied MTSET would have to gain access to the cysteine side chain of N14C through the pore. However, N14C hemichannels are effectively nonconducting. The charge of MTSEA, though, depends on pH with the pK_a of the amine group estimated to be ~8.5 (Karlin and Akabas, 1998). Thus, deprotonated forms of MTS EA can permeate the membrane and modify N14C in the absence of an open hemichannel pore.

Because accessibility of MTSEA, due to its membrane permeability, does not identify N14 as pore lining, we reexamined accessibility of the membrane-impermeant MTSET reagent in oocytes co-injected with N14C and WT Cx26 in attempts to improve the function of hemichannels containing N14C subunits. Whereas application of MTSET at a holding potential of −40 mV had little effect in oocytes expressing N14C alone, co-injected oocytes showed a substantial increase in current consistent with gained access for MTSET (Fig. 8 B). After exposure to MTSET for ~2–3 min, subsequent application of MTSEA further increased the current, but the increase tended to be smaller than the effects of MTSEA in oocytes that had no prior exposure to MTS ET. These results suggest heteromeric hemichannels open sufficiently, allowing MTSET to enter the pore and modify cysteine side chains, leaving less N14C subunits available for modification by MTSEA upon subsequent application. The converse order of application showed no effect of MTSET after exposure to MTSEA for ~2–3 min (Fig. 8 C), indicating that MTSEA can effectively modify all N14C subunits within this time frame. Of note, application of MTSET to hemichannels containing N14C subunits, whether homomeric or heteromeric with WT Cx26, increased currents to a larger extent at depolarizing potentials, a condition that also promoted hemichannel opening (Fig. S1). These data demonstrate that the membrane-impermeant MTSET reagent added to the extracellular side can modify N14C, which is located on the cytoplasmic N terminus, when hemichannel opening is induced, consistent with access to the residue via the aqueous pore.

We also examined the effects of other MTS reagents that would render the side chain at N14C negatively

Downloaded from http://rupress.org/jgp/article-pdf/148/1/25/1795860/jgp_201611585.pdf by guest on 04 December 2025

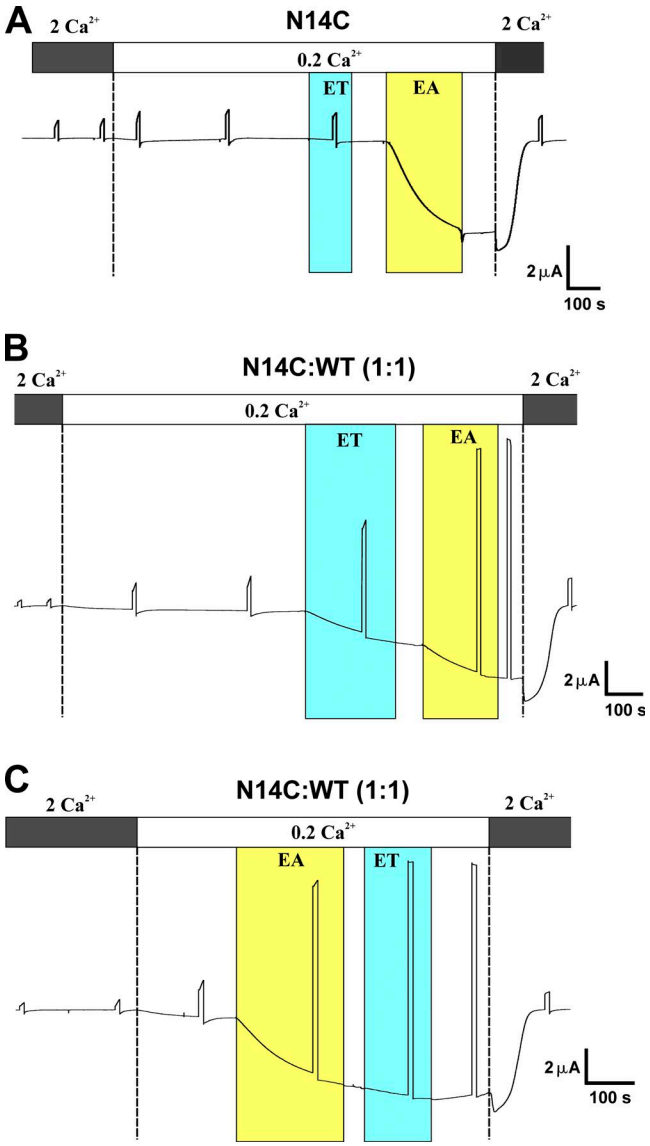

Figure 8. **Substituted cysteine accessibility supports exposure of N14 to the aqueous pore.** (A–C) Shown are effects of MTSEA and MTSET on macroscopic currents recorded from oocytes expressing N14C alone (A) or co-injected with WT Cx26 (B and C). Oocytes were bathed in a simple 100 mM NaCl salt solution containing the indicated Ca^{2+} concentrations and held at −40 mV throughout except for periodic steps to 40 mV to assess hemichannel activation at a positive voltage. (A) Responses of N14C to MTSET and MTSES. Bath application of MTSET showed little or no effect, whereas subsequent application of MTSEA produced a large induction of current. (B) The same experiment as in A, except it was performed in a cell co-injected with N14C and WT Cx26 in a 1:1 ratio. Bath application of MTS ET induced an increase in current, and the subsequent action of MTSEA was attenuated. (C) In a cell co-injected with N14C and WT Cx26 in a 1:1 ratio, bath application of MTSEA induced a large current that occluded the subsequent action of MTS ET, indicating that the same site is modified by both reagents and that MTSEA modifies all available sites. MTS reagents are designated as ET for MTSET and EA for MTSEA.

charged (MTSES) or neutral, but bulky (MTSEA biotin-XX). MTSES showed little effect on currents in cells co-injected with N14C and WT (1:1), and subsequent application of MTSET and MTSEA still substantially increased currents, indicating that limited, if any, modification by MTSES had occurred (Fig. 9 A). However, MTSEA biotin-XX produced a substantial increase in current over 2–3 min, and the effect of a subsequently applied MTS reagent was markedly reduced (Fig. 9 B). The same was true for MTSEA biotin and MTSEA biotin-X (not depicted). The increase in current produced by MTSEA, MTSET, MTSES, and MTSEA biotin-XX reagents in oocytes expressing N14C and N14C + WT is summarized in Fig. 9 C. The fraction of the total current increase produced by MTSEA after application by MTSET, MTSES, or MTSEA biotin-XX is summarized in Fig. 9 D.

Although application of MTS biotin reagents increased N14C currents, suggesting modification of the side chain that contains a biotin moiety improves function, the hemichannels behaved differently from those in which the side chain was modified to a positive charge by MTSEA or MTSET. N14C hemichannels modified to a positive charge with MTSEA exhibited little gating with hyperpolarization in low extracellular Ca^{2+} much like N14K hemichannels, consistent with stabilization of the open state. N14C hemichannels modified by MTS ET also exhibited impaired gating at negative potentials but did show some modest reductions in current. However, N14C hemichannels modified by MTSEA biotin-XX continued to show strong gating with hyperpolarization (Fig. 10 A). Thus, rescue of N14C hemichannel function can occur upon modification by very different MTS reagents, but the stably open phenotype appears to be a property associated with positive charge at N14.

Given that modification by MTSEA biotin-XX improves hemichannel function, we recorded from single hemichannels to assess effects on unitary conductance. Much to our surprise, despite the introduction of bulky side chains into the pore, the unitary conductance of an N14C hemichannel modified by MTSEA biotin-XX was only slightly reduced (328 ± 16) compared with WT Cx26 (340 ± 9), although open hemichannel noise appeared elevated (Fig. 10 B).

The N14K gating phenotype; possible role of intersubunit NT–TM2 interactions

Because the stably open gating phenotype appears to be associated with a positive charge at the N14 position, we examined the crystal structure to identify potential underlying electrostatic interactions. In the structure, N14 is situated on a loop connecting a short NT helix with the TM1 helix and is in close proximity to a segment in the adjacent subunit, designated as the cytoplasmic extension of TM2 (Maeda et al., 2009). This region was

Downloaded from http://rupress.org/jgp/article-pdf/148/1/25/1795860/jgp_201611585.pdf by guest on 04 December 2025

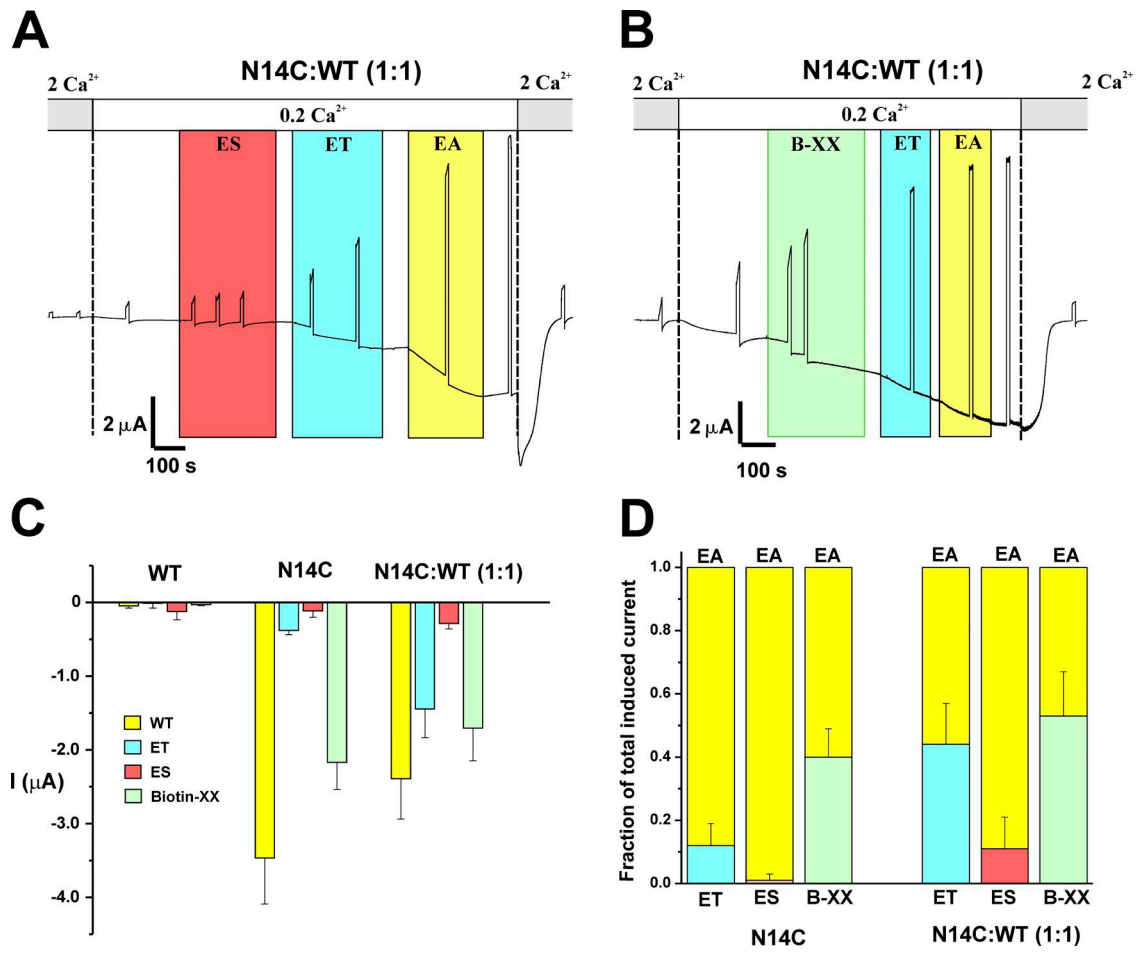

Figure 9. **Effects of MTS reagents on Cx26 hemichannels containing N14C subunits.** (A) Bath application of the negatively charged MTSES reagent (ES) to a cell co-injected with N14C and WT Cx26 in a 1:1 ratio did not significantly affect current. Subsequent actions of MTS reagents were not affected. (B) Bath application of MTSEA biotin-XX to cells co-injected with N14C and WT Cx26 in a 1:1 ratio induced current. Subsequent actions of MTSET and MTSEA were attenuated. (C) Bar graph summarizing the effects of MTS reagents on oocytes injected with N14C and N14C + WT (1:1). Values represent the mean change in current in 0.2 mM Ca^{2+} after a 3-min exposure to MTSEA (yellow), MTSET (cyan), MTSES (red), and MTS biotin-XX (green). Error bars represent ±SEM; the number of oocytes tested ranged from five to nine. (D) Bar graph summarizing the effect of MTSET, MTSEA, or MTS biotin-XX application on a subsequent MTSEA application. MTSET, MTSEA, or MTS biotin-XX was applied for 3 min and followed by exposure to MTSEA for 3 min. The current after exposure to MTSEA was designated as the total current. Colored portions of each bar represent the fraction of the total current produced by the indicated MTS reagent. Co-injected oocytes show an increase in the fraction of the total current produced by MTSET or MTS biotin-XX, indicating that the N14C subunit is modified, leaving less available for subsequent MTSEA modification. Values represent mean ± SEM; the number of oocytes ranged from 6 to 10. MTS reagents were designated as ET for MTSET, EA for MTSEA, ES for MTSES, and B-XX for MTSEA biotin-XX.

formerly assigned to the cytoplasmic loop domain (Bennett et al., 1991) and is highly charged with a sequence of RRHEKKRK (residues 98–105). A high content of charged residues in this region is common among connexin isoforms, although the exact sequence is quite variable.

A putative residue in TM2 that may come in close proximity to N14 is H100 (Fig. 11 A). A histidine residue in its unprotonated form can act as the aromatic motif in a cation–π interaction (Liao et al., 2013), suggesting the possibility of an electrostatic H100–N14K interaction. Thus, as a first step, we created a double mutant (N14K + H100A). The G-V relationship in 0.2 mM Ca^{2+} of the double mutant resembled that of WT Cx26 (Fig. 11 B). Substitution of alanine alone at H100 also resembled WT Cx26, suggesting that the H100A substitution did not significantly impact hemichannel structure and, thus, was unlikely to exert an effect on N14K allosterically in the double mutant. In addition to restored loop gating, sensitivity to pH was restored (Fig. 11 C). Thus, in the presence of an H100A substitution, the N14K mutation no longer rendered the hemichannel refractory to closure by pH and by voltage via loop gating in low Ca^{2+} conditions. Substitution of alanine alone at N14, which also would preclude interaction with H100, resulted in impaired hemichan-

Downloaded from http://rupress.org/jgp/article-pdf/148/1/25/1795860/jgp_201611585.pdf by guest on 04 December 2025

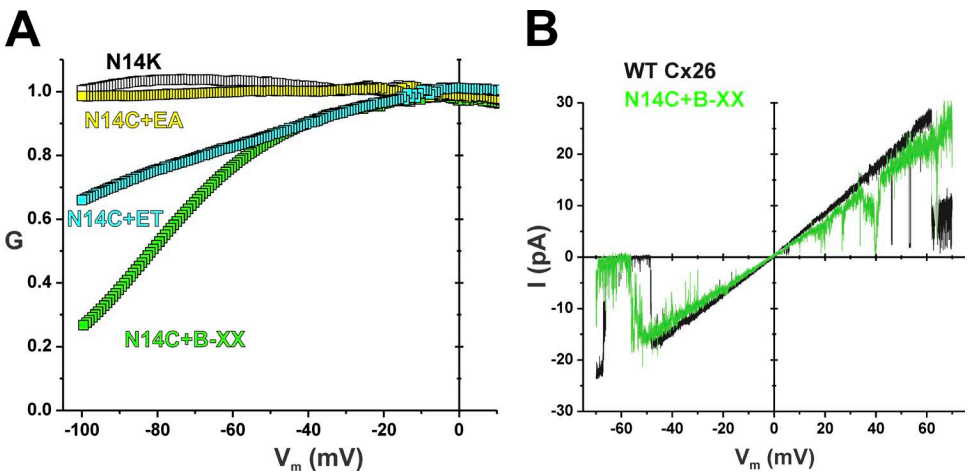

Figure 10. **Effects of MTS reagents on Cx26 hemichannels containing N14C subunits on gating and unitary conductance.** (A) Superimposed normalized G-V relationships of N14K hemichannels (open symbols) and N14C hemichannels modified by MTSEA (yellow symbols), MTSET (cyan symbols), and MTSEA biotin-XX (green symbols). Recordings were performed in 0.2 mM Ca^{2+}. MTS reagents were applied for 10 min before obtaining the G-V relationships via slow (600 s) voltage ramps between 40 and −100 mV from a holding potential of −20 mV. Data points represent mean values. Error bars were omitted for clarity. N14C + MTSEA, n = 3; N14C + MTSET, n = 4; N14C + MTSEA biotin-XX, n = 5. Data for N14K is the same as in Fig. 2. (B) Superimposed patch clamp recordings from cell-attached patches containing a single WT Cx26 hemichannel and a single N14C hemichannel modified by MTS EA biotin-XX. Currents were obtained by applying 8-s voltage ramps between 70 and −70 mV and leak subtracted (see Materials and methods). The N14C hemichannel modified by MTSEA biotin-XX was only slightly reduced in conductance and exhibited a noisier and a more flickery open hemichannel current. Bath and pipette solutions consisted of IPS (see Materials and methods). Data were acquired at 5 kHz and filtered at 1 kHz. MTS reagents were designated as ET for MTSET, EA for MTSEA, and B-XX for MTSEA biotin-XX.

nel function, much like N14Y and N14C; MTS reagents had no effect on N14A or N14Y hemichannels. These data implicate an electrostatic NT–TM2 interaction in the expression of the N14K gating phenotype but also show that substitutions at N14 can differentially impact hemichannel function.

DISCUSSION

Aberrant Cx26 hemichannels are a common feature of KID syndrome, as well as other Cx26-asscociated deafness syndromes, and there is growing evidence that differences in biophysical properties of mutant hemichannels underlie the phenotypic diversity exhibited among patients (Sanchez and Verselis, 2014). Here, we find that two mutations at the same position of Cx26, N14K and N14Y, which have been reported to produce different phenotypes (de Zwart-Storm et al., 2011), generate hemichannels that differ substantially in their biophysical properties, strengthening the link between aberrant hemichannel function and disease pathogenesis in Cx26-mediated syndromic deafness.

Differential effects of N14 syndromic deafness mutants on hemichannel function

Both N14K and N14Y mutations produce functional hemichannels, but currents associated with N14Y typically were very small regardless of the extracellular Ca^{2+} concentration when expressed alone or together with WT Cx26. N14K currents were robust in low Ca^{2+} but were strongly inhibited in 2 mM Ca^{2+} much like WT Cx26. These differences alone suggest that the mechanisms of disease pathogenesis involving N14K and N14Y hemichannels are likely to differ. N14K and N14Y mutations also substantially affected loop gating, which mediates hemichannel opening in the plasma membrane (Trexler et al., 1996). Again, the effects of the two mutations on loop gating differed substantially, essentially producing opposite shifts in voltage-dependent activation, negative for N14K and positive for N14Y. In low Ca^{2+} conditions, N14K hemichannels showed a loss of gating, leaving them in a stably open configuration, whereas N14Y hemichannels continued to gate strongly. Finally, pH, which robustly regulates Cx26 hemichannels in a physiological range (Sanchez et al., 2014), was rendered ineffective in N14K and less effective in N14Y. Overall, the effects on loop gating and regulation by pH further enhance the differential functional efficiencies exhibited by these two mutants.

Loop gating and intersubunit interactions between NT and TM2 domains

When examined at the single-channel level, N14K remarkably resulted in hemichannels that essentially remained open in low Ca^{2+} conditions, with no evidence of stable closing events, even when large hyperpolarizing voltages were applied. This behavior contrasts WT Cx26 and several other KID mutants we examined such

Downloaded from http://rupress.org/jgp/article-pdf/148/1/25/1795860/jgp_201611585.pdf by guest on 04 December 2025

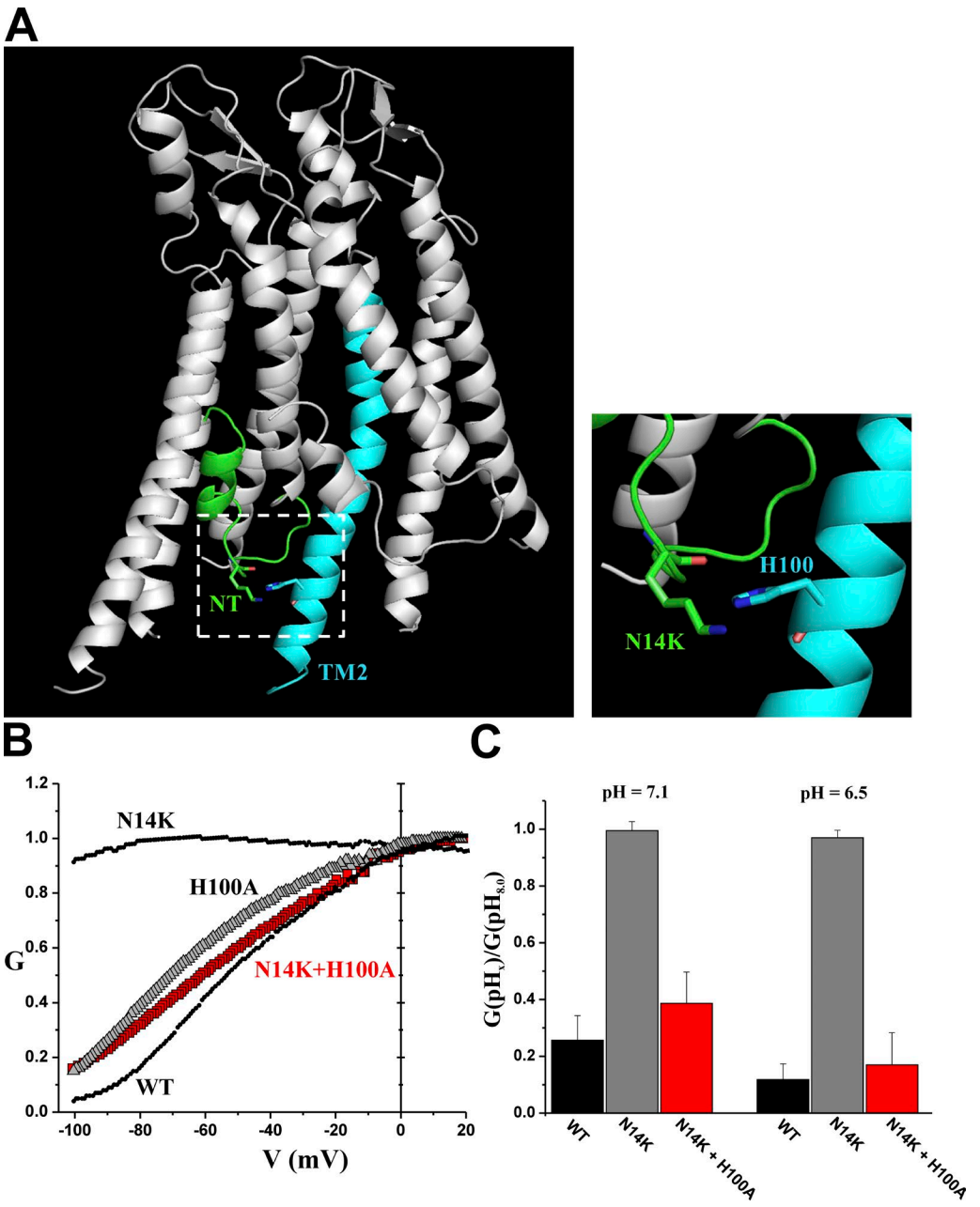

Figure 11. **The double mutant N14K + H100A reverses the gating and pH phenotypes caused by N14K.** (A) Representation of two adjacent hemichannel subunits from the atomic structure of Cx26 (Protein Data Bank accession no. 2ZW3; Maeda et al., 2009). The structure is displayed using the PyMOL Molecular Graphics System. The N terminus (NT) of one subunit (green) comes into close proximity to the cytoplasmic extension of the TM2 domain of an adjacent subunit (cyan). The N14K mutated residue in the N terminus is shown in close association with H100 in TM2 (inset shows an expanded view). The position of the mutated residue lysine at position 14 was selected from a set of backbone-dependent rotamers. (B) Superimposed normalized G-V relationships of N14K and WT Cx26 are shown (black) together with the double mutant N14K + H100A (red symbols) and H100A (open symbols) alone. The double N14K + H100A mutation resembles WT Cx26, suggesting that N14K and H100 may interact to stabilize opening in N14K hemichannels, making them refractory to gating upon hyperpolarization. Recordings were performed in 0.2 mM Ca^{2+}. G-V relationships were obtained by applying slow (600 s) voltage ramps between 40 and −100 mV from a holding potential of −20 mV. Each point is the mean conductance. Error bars were omitted for clarity. H100A, n = 4; N14K + 100A, n = 7. Data for N14K and WT are the same as in Fig. 2. (C) The loss of sensitivity to pH caused by the N14K mutation is also reversed in the double N14K + H100A mutant. Bar graph comparing pH responses of WT Cx26, N14K, and N14K + H100A hemichannels. Shown are data for pH 7.1 and 6.5 plotted as the ratios of the macroscopic conductances at each of these two pH values relative to pH 8.0. Conductance was calculated from oocytes held at −40 mV. Each bar represents the mean ratio ± SEM. N14K + H100A, n = 10. Data for WT Cx26 and N14K are the same as in Fig. 6.

Downloaded from http://rupress.org/jgp/article-pdf/148/1/25/1795860/jgp_201611585.pdf by guest on 04 December 2025

as A40V, G45E, and D50N, in which loop gating remains active at all voltages and is biased toward closure with hyperpolarization. N14K hemichannels continued to exhibit active flickering events from the open state. These events, when examined at a higher time resolution, did not reach a steady current sublevel and, like for WT Cx26 hemichannels, may represent incomplete attempts at closure. Nonetheless, the long-lived stable closures were absent in N14K hemichannels, which together with slow kinetics of macroscopic current decay suggest a stabilization of the open state for the loop gating mechanism. Although current levels were low and we could not obtain unitary events for N14Y hemichannels, we reason that the opposite is likely true, i.e., the open state is destabilized, as suggested by the considerably faster kinetics with which conductance decreased on hyperpolarization in macroscopic recordings. The other gating mechanism, V_j or fast gating, which closes Cx26 hemichannels to a stable substate at positive membrane potentials, remained, and G-V curves derived from ensembles of voltage ramps were similar to WT Cx26. Thus, the N14K mutation has a robust effect on loop gating but appears to minimally impact V_j gating.

N14K represents a charge substitution and mechanistically we explored the possibility of an intersubunit electrostatic interaction to explain the effect on the loop gating mechanism. As suggested by the crystal structure, N14K and H100 may be in close proximity and can plausibly interact in a cation–π configuration, with the imidazole side chain of histidine in its unprotonated form acting as the aromatic motif. Although not common, this type of cation–π interaction has been described in proteins (Reddy and Sastry, 2005; Liao et al., 2013). Such an interaction should be disrupted by acidification via protonation of the histidine residue, but we saw no effect on the N14K mutant hemichannel down to pH 6.5; acidification of oocytes <6.5 compromised cell integrity. This lack of a noticeable effect down to pH 6.5 is not surprising given that the pK_a of the imidazole side chain of a histidine residue in solution is ∼6.0 and can be shifted even more acidic when incorporated into a protein. Substantial shifts in pK_a values have been demonstrated for several titratable residues in native proteins (Cymes and Grosman, 2011a,b).

We point out that there appear to be two effects of substitutions at N14. Substitution with alanine, cysteine, as well as the disease-causing tyrosine resulted in small currents indicative of considerably impaired hemichannel function. N14K and modification of N14C to a positive charge with MTS reagents exhibited large currents and stably open hemichannels, suggesting an electrostatic effect, possibly through interaction with H100 as described. However, the N14K + H100A double mutant, which prevents this particular electrostatic interaction, still resulted in robust hemichannel currents. Moreover, modification of N14C by MTS biotin reagents, which result in bulky, neutral side chains that would not interact electrostatically with H100, also produced large currents. However, the N14K + H100A double mutant and N14C mutants modified with MTS biotin reagents retained strong loop gating upon hyperpolarization in low Ca^{2+}. Thus, the nature of the substitution at the N14 position can result in impaired or robust hemichannel function, but robust function can be separate from the stably open gating phenotype, which appears to be an electrostatic effect associated with positive charge at N14.

Ultimately, we have no direct evidence of the nature of the interaction involving N14K that leads to stabilization of the open state. It is possible that N14K interacts with a residue other than H100 in an attractive or repulsive manner. Also, it is possible that N14K is not directly involved in an electrostatic interaction but alters the structure of the NT domain, leading to alterations in other interactions. The structure of the NT domain has been shown to be critical to connexin channel function and very sensitive to amino acid substitutions (Purnick et al., 2000a; Kyle et al., 2008, 2009; Kalmatsky et al., 2012). Specifically for Cx26, the impact of the N14Y substitution on NT structure using nuclear magnetic resonance (NMR) spectroscopy reported a change in the flexibility of the NT domain, which could significantly affect channel function (Arita et al., 2006). Thus, N14Y and N14K may affect the structure of NT in different ways, explaining the differential effects on the levels of expressed currents and gating, which may very well involve interactions between NT and TM2 domains involving residues that constitute the region of high charge density in TM2. Resolution of the potentially complex set of interactions in this region of Cx26 will require extensive mutagenesis coupled with molecular modeling.

The NT domain and loop gating

Earlier studies of loop (slow) gating and V_j (fast) gating suggested that the two distinct forms of gating may be localized at opposite ends of a connexin hemichannel in the cytoplasmic NT domain for V_j gating and the extracellular loop domains for loop gating (Verselis et al., 1994, 2009; Oh et al., 2000; Purnick et al., 2000b; Bukauskas and Verselis, 2004; Tang et al., 2009). The N14K mutation had a profound effect on loop gating, essentially eliminating stable closing events in low extracellular Ca^{2+} conditions. V_j gating essentially remained unaffected.

Given the association of V_j gating and the N terminus, the profound effect on the loop gating mechanism caused by the N14K mutation was somewhat surprising. However, more recent studies have indicated that loop gating involves conformational changes at the cytoplasmic as well as the extracellular ends of the hemichannel. In Cx50 hemichannels, *N*-benzylquininium, the quaternary derivative of quinine, was reported to produce inhibition by binding to the NT domain and pro-

Downloaded from http://rupress.org/jgp/article-pdf/148/1/25/1795860/jgp_201611585.pdf by guest on 04 December 2025

moting closure of the loop gate (Rubinos et al., 2012). Thus, conformational changes in NT, presumably caused by drug binding, appear to affect loop gating. Also, examination of metal bridge formation between substituted cysteines in the Cx32*43E1 chimeric hemichannel suggest that the cytoplasmic entrance to the pore, constituted by NT, may narrow with loop gating through alteration of the TM1/E1 bend angle via reorganization of electrostatic interactions in the parahelical domain at the extracellular membrane border (Kwon et al., 2013). The effect of N14 KID mutants on loop gating supports these latter views.

One of the interesting observations we report here is that loop gating in Cx26 hemichannels appears to have a constitutive component. In low Ca^{2+} conditions, macroscopic conductance is maximal and remains constant over a wide voltage range, yet recordings of single hemichannels show active loop gating transitions in this voltage range. Interestingly, this behavior is not observed in Cx46 and Cx50 hemichannels, which remain stably open in low Ca^{2+} conditions at voltages where macroscopic conductance remains constant and closed with robust hyperpolarization (Trexler et al., 1996; Srinivas et al., 2005). Thus, it may be that the loop gating properties of connexin hemichannels are determined by specific intersubunit interactions between NT and TM2 domains that differentially stabilize the open state, thereby regulating hemichannel closure with hyperpolarization. It is interesting that the cytoplasmic extension of TM2 is highly charged in all connexins, which may signify a motif that is important for defining the properties of loop gating.

N14 syndromic deafness mutants and effects on Ca^{2+} and pH on Cx26 hemichannels

Studies have suggested that both pH and extracellular Ca^{2+} act on connexin hemichannels by modulating loop gating (Trexler et al., 1996, 1999; Verselis and Srinivas, 2008; Sanchez et al., 2014). In this view, closure of the loop gate can be promoted by the binding of Ca^{2+} and/or by titration of relevant amino acid residues (Trexler et al., 1999; Sanchez et al., 2014). Because N14K stabilizes the open state of loop gating, we reasoned that closure of the loop gate by Ca^{2+} and pH also may be affected. Although extracellular Ca^{2+} continued to be effective at closing N14K hemichannels, the kinetics of Ca^{2+} inhibition was slowed, indicating that the action of Ca^{2+} was altered in some way (Fig. S2). We were unable to obtain a dose–response curve for Ca^{2+}, as the slow kinetics of closure prolonged Ca^{2+} influx upon addition of Ca^{2+} to the bath, which irreversibly reduced currents, perhaps by promoting connexin internalization. In any case, the retained ability of Ca^{2+} to inhibit N14K hemichannels indicates that the binding of Ca^{2+} can overcome the conformational stability induced by the N14K mutation. However, titration of residues with acidification does not appear to be able to overcome this conformational stability, leaving N14K hemichannels refractory to pH, at least down to pH 6.5. Thus, despite their common action on the loop gate, Ca^{2+} and pH are differentially affected by the N14K mutation by virtue of their actions at separate sites, which appear to promote different conformational pathways leading to closure of the loop gate.

N14 is exposed to the hemichannel pore

Our data here are consistent with exposure of N14 to the aqueous pore in general agreement with the Cx26 crystal structure. This conclusion is based on our ability to modify N14C subunits with bath application of the membrane-impermeant MTSET reagent only when hemichannel opening was induced, either by prolonged depolarization and/or coexpression of N14C with WT. For a residue facing an aqueous environment, it was surprising that the N14K substitution did not affect unitary conductance and that replacement of N14 with cysteine, alanine, or tyrosine residues resulted in poor hemichannel function. For the latter, as previously discussed, the conformation of NT appears to be very sensitive to amino acid substitutions, thereby potentially inducing robust but differential effects depending on the particular substitution. For the N14K hemichannel, an electrostatic interaction with another residue, which likely explains the stabilization of the open state, can also reduce the impact of a positive charge substitution in the pore, thereby explaining the lack of a measureable effect on unitary conductance. Also, as the crystal structure suggests, N14K is likely located in a wide region of the pore, which also can explain the lack of an appreciable effect on unitary conductance, with narrowed regions in other locations of the pore largely governing the rate of ion flux. In support, introduction of bulky side chains at this position by modifying N14C with MTSEA biotin-XX did not appreciably reduce unitary conductance.

N14K and N14Y and their potential effects in cochlea and skin

Loss of Cx26, the most prevalent cause of nonsyndromic deafness, does not produce skin disorders. Thus, syndromic mutants appear to be gain-of-function mutants, and aberrantly functioning hemichannels are a common property, particularly in KID syndrome (Lee and White, 2009; Xu and Nicholson, 2013; Sanchez and Verselis, 2014). Interestingly, hemichannels containing N14K subunits residing in cochlear-supporting cell membranes exposed to the endolymphatic compartment, which is low in Ca^{2+}, would tend to be particularly refractory to closure even with the large hyperpolarized voltage imposed by the endolymphatic potential. In addition, the striking loss of regulation by pH could promote more opening of N14K hemichannels, even those

Downloaded from http://rupress.org/jgp/article-pdf/148/1/25/1795860/jgp_201611585.pdf by guest on 04 December 2025

located in basolateral membranes exposed to normal extracellular Ca^{2+}. This added opening would be exacerbated in an acidic environment, such as the buccal mucosa (Aframian et al., 2006), perhaps explaining the unusual mucocutaneous manifestations described in patients carrying the N14K mutation (van Steensel et al., 2004; Lazic et al., 2008).

N14Y, however, appears to be poorly functional as a hemichannel and exhibits shifted gating that further reduces opening at hyperpolarized voltages, indicating that a simple gain-of-function model for hemichannels may not apply in this case. However, recent findings suggest that the S17F KID syndrome mutation in the NT domain, which lacks function as a hemichannel and a GJ channel, may cause skin pathology by inducing opening of heteromeric hemichannels by aberrantly interacting with Cx43, which is also expressed in keratinocytes (García et al., 2015). The same study suggested a similar possibility for N14Y, although the properties of these heteromeric hemichannels with Cx43 have not been fully characterized. Oligomerization is a complex process, and several connexin domains have been implicated (Lagree et al., 2003; Gemel et al., 2006; Martínez et al., 2011; Smith et al., 2012; Koval et al., 2014). Studies in Cx26 suggest that residues in TM1 regulate oligomerization (Jara et al., 2012) but do not rule out additional steps involving the NT domain (García et al., 2015). Of note, heterooligomerization into hexamers does not necessarily lead to functional channels, and it will be interesting to see to what extent NT structure and NT–TM2 interactions can regulate these processes in Cx26.

For either N14K or N14Y, our data showing exposure of N14 to the pore of open hemichannels suggest that these mutations have the potential to affect hemichannel permeability. Although we did not observe a change in unitary conductance carried by K^+ and Cl^-, larger molecules, such as ATP or metabolites, could be affected and contribute to disease pathogenesis.

Our studies of N14 mutants in *Xenopus* oocytes reveal possible differences in hemichannel properties that may determine the disease phenotypes in patients, but it remains to be determined how the mutant hemichannels express, traffic, and function in native tissues. There are also potential contributions of GJ channels. Studies, thus far, have not provided a consensus regarding GJ channel function for N14K and N14Y mutants. N14K, which showed coupling between pairs of oocytes, failed to show dye transfer between transfected HeLa cells (Lee et al., 2009; de Zwart-Storm et al., 2011). Keratinocytes isolated from a patient carrying the N14Y mutation showed dye spread, albeit reduced compared with normal keratinocytes, suggesting a negative impact on GJ channel function (Arita et al., 2006). No studies have examined GJ permeability, particularly given our evidence that N14 is pore lining. Thus, although aberrant hemichannel function plausibly plays a central role, GJs cannot be ruled out as contributors to disease pathogenesis in KID syndrome mutants.

ACKNOWLEDGMENTS

This work was supported by National Institutes of Health grants GM54179 to V.K. Verselis and EY013869 to M. Srinivas. H.A. Sanchez was supported by National Institutes of Health training grant T32 NS007439.

The authors declare no competing financial interests.

Angus C. Nairn served as editor.

Submitted: 16 February 2016
Accepted: 10 June 2016

REFERENCES

Aframian, D.J., T. Davidowitz, and R. Benoliel. 2006. The distribution of oral mucosal pH values in healthy saliva secretors. *Oral Dis.* 12:420–423. http://dx.doi.org/10.1111/j.1601-0825.2005.01217.x

Arita, K., M. Akiyama, T. Aizawa, Y. Umetsu, I. Segawa, M. Goto, D. Sawamura, M. Demura, K. Kawano, and H. Shimizu. 2006. A novel N14Y mutation in Connexin26 in keratitis-ichthyosis-deafness syndrome: analyses of altered gap junctional communication and molecular structure of N terminus of mutated Connexin26. *Am. J. Pathol.* 169:416–423. http://dx.doi.org/10.2353/ajpath.2006.051242

Bennett, M.V., L.C. Barrio, T.A. Bargiello, D.C. Spray, E. Hertzberg, and J.C. Sáez. 1991. Gap junctions: new tools, new answers, new questions. *Neuron.* 6:305–320. http://dx.doi.org/10.1016/0896-6273(91)90241-Q

Bukauskas, F.F., and V.K. Verselis. 2004. Gap junction channel gating. *Biochim. Biophys. Acta.* 1662:42–60. http://dx.doi.org/10.1016/j.bbamem.2004.01.008

Coggshall, K., T. Farsani, B. Ruben, T.H. McCalmont, T.G. Berger, L.P. Fox, and K. Shinkai. 2013. Keratitis, ichthyosis, and deafness syndrome: a review of infectious and neoplastic complications. *J. Am. Acad. Dermatol.* 69:127–134. http://dx.doi.org/10.1016/j.jaad.2012.12.965

Cymes, G.D., and C. Grosman. 2011a. Estimating the pKa values of basic and acidic side chains in ion channels using electrophysiological recordings: a robust approach to an elusive problem. *Proteins.* 79:3485–3493. http://dx.doi.org/10.1002/prot.23087

Cymes, G.D., and C. Grosman. 2011b. Tunable pKa values and the basis of opposite charge selectivities in nicotinic-type receptors. *Nature.* 474:526–530. http://dx.doi.org/10.1038/nature10015

de Zwart-Storm, E.A., R.F. Rosa, P.E. Martin, R. Foelster-Holst, J. Frank, A.E. Bau, P.R. Zen, C. Graziadio, G.A. Paskulin, M.A. Kamps, et al. 2011. Molecular analysis of connexin26 asparagine14 mutations associated with syndromic skin phenotypes. *Exp. Dermatol.* 20:408–412. http://dx.doi.org/10.1111/j.1600-0625.2010.01222.x

García, I.E., J. Maripillán, O. Jara, R. Ceriani, A. Palacios-Muñoz, J. Ramachandran, P. Olivero, T. Perez-Acle, C. González, J.C. Sáez, et al. 2015. Keratitis-ichthyosis-deafness syndrome-associated Cx26 mutants produce nonfunctional gap junctions but hyperactive hemichannels when co-expressed with wild type Cx43. *J. Invest. Dermatol.* 135:1338–1347. http://dx.doi.org/10.1038/jid.2015.20

Gemel, J., X. Lin, R.D. Veenstra, and E.C. Beyer. 2006. N-terminal residues in Cx43 and Cx40 determine physiological properties of gap junction channels, but do not influence heteromeric assembly with each other or with Cx26. *J. Cell Sci.* 119:2258–2268. http://dx.doi.org/10.1242/jcs.02953

Downloaded from http://rupress.org/jgp/article-pdf/148/1/25/1795860/jgp_201611585.pdf by guest on 04 December 2025

Gerido, D.A., A.M. DeRosa, G. Richard, and T.W. White. 2007. Aberrant hemichannel properties of Cx26 mutations causing skin disease and deafness. *Am. J. Physiol. Cell Physiol.* 293:C337–C345. http://dx.doi.org/10.1152/ajpcell.00626.2006

Jara, O., R. Acuña, I.E. García, J. Maripillán, V. Figueroa, J.C. Sáez, R. Araya-Secchi, C.F. Lagos, T. Pérez-Acle, V.M. Berthoud, et al. 2012. Critical role of the first transmembrane domain of Cx26 in regulating oligomerization and function. *Mol. Biol. Cell.* 23:3299–3311. http://dx.doi.org/10.1091/mbc.E11-12-1058

Kalmatsky, B.D., Y. Batir, T.A. Bargiello, and T.L. Dowd. 2012. Structural studies of N-terminal mutants of connexin 32 using (1)H NMR spectroscopy. *Arch. Biochem. Biophys.* 526:1–8. http://dx.doi.org/10.1016/j.abb.2012.05.027

Karlin, A., and M.H. Akabas. 1998. Substituted-cysteine accessibility method. *Methods Enzymol.* 293:123–145. http://dx.doi.org/10.1016/S0076-6879(98)93011-7

Koval, M., S.A. Molina, and J.M. Burt. 2014. Mix and match: investigating heteromeric and heterotypic gap junction channels in model systems and native tissues. *FEBS Lett.* 588:1193–1204. http://dx.doi.org/10.1016/j.febslet.2014.02.025

Kronengold, J., E.B. Trexler, F.F. Bukauskas, T.A. Bargiello, and V.K. Verselis. 2003. Single-channel SCAM identifies pore-lining residues in the first extracellular loop and first transmembrane domains of Cx46 hemichannels. *J. Gen. Physiol.* 122:389–405. http://dx.doi.org/10.1085/jgp.200308861

Kwon, T., Q. Tang, and T.A. Bargiello. 2013. Voltage-dependent gating of the Cx32*43E1 hemichannel: conformational changes at the channel entrances. *J. Gen. Physiol.* 141:243–259. http://dx.doi.org/10.1085/jgp.201210839

Kyle, J.W., P.J. Minogue, B.C. Thomas, D.A. Domowicz, V.M. Berthoud, D.A. Hanck, and E.C. Beyer. 2008. An intact connexin N-terminus is required for function but not gap junction formation. *J. Cell Sci.* 121:2744–2750. http://dx.doi.org/10.1242/jcs.032482

Kyle, J.W., V.M. Berthoud, J. Kurutz, P.J. Minogue, M. Greenspan, D.A. Hanck, and E.C. Beyer. 2009. The N terminus of connexin37 contains an alpha-helix that is required for channel function. *J. Biol. Chem.* 284:20418–20427. http://dx.doi.org/10.1074/jbc.M109.016907

Lagree, V., K. Brunschwig, P. Lopez, N.B. Gilula, G. Richard, and M.M. Falk. 2003. Specific amino-acid residues in the N-terminus and TM3 implicated in channel function and oligomerization compatibility of connexin43. *J. Cell Sci.* 116:3189–3201. http://dx.doi.org/10.1242/jcs.00604

Lazic, T., K.A. Horii, G. Richard, D.I. Wasserman, and R.J. Antaya. 2008. A report of GJB2 (N14K) Connexin 26 mutation in two patients—a new subtype of KID syndrome?. *Pediatr. Dermatol.* 25:535–540. http://dx.doi.org/10.1111/j.1525-1470.2008.00767.x

Lee, J.R., and T.W. White. 2009. Connexin-26 mutations in deafness and skin disease. *Expert Rev. Mol. Med.* 11:e35. http://dx.doi.org/10.1017/S1462399409001276

Lee, J.R., A.M. Derosa, and T.W. White. 2009. Connexin mutations causing skin disease and deafness increase hemichannel activity and cell death when expressed in *Xenopus* oocytes. *J. Invest. Dermatol.* 129:870–878. http://dx.doi.org/10.1038/jid.2008.335

Liao, S.M., Q.S. Du, J.Z. Meng, Z.W. Pang, and R.B. Huang. 2013. The multiple roles of histidine in protein interactions. *Chem. Cent. J.* 7:44. http://dx.doi.org/10.1186/1752-153X-7-44

Maeda, S., S. Nakagawa, M. Suga, E. Yamashita, A. Oshima, Y. Fujiyoshi, and T. Tsukihara. 2009. Structure of the connexin 26 gap junction channel at 3.5 A resolution. *Nature.* 458:597–602. http://dx.doi.org/10.1038/nature07869

Martínez, A.D., J. Maripillán, R. Acuña, P.J. Minogue, V.M. Berthoud, and E.C. Beyer. 2011. Different domains are critical for oligomerization compatibility of different connexins. *Biochem. J.* 436:35–43. http://dx.doi.org/10.1042/BJ20110008

Oh, S., J.B. Rubin, M.V. Bennett, V.K. Verselis, and T.A. Bargiello. 1999. Molecular determinants of electrical rectification of single channel conductance in gap junctions formed by connexins 26 and 32. *J. Gen. Physiol.* 114:339–364. http://dx.doi.org/10.1085/jgp.114.3.339

Oh, S., C.K. Abrams, V.K. Verselis, and T.A. Bargiello. 2000. Stoichiometry of transjunctional voltage-gating polarity reversal by a negative charge substitution in the amino terminus of a connexin32 chimera. *J. Gen. Physiol.* 116:13–32. http://dx.doi.org/10.1085/jgp.116.1.13

Pfahnl, A., and G. Dahl. 1998. Localization of a voltage gate in connexin46 gap junction hemichannels. *Biophys. J.* 75:2323–2331. http://dx.doi.org/10.1016/S0006-3495(98)77676-3

Purnick, P.E., D.C. Benjamin, V.K. Verselis, T.A. Bargiello, and T.L. Dowd. 2000a. Structure of the amino terminus of a gap junction protein. *Arch. Biochem. Biophys.* 381:181–190. http://dx.doi.org/10.1006/abbi.2000.1989

Purnick, P.E., S. Oh, C.K. Abrams, V.K. Verselis, and T.A. Bargiello. 2000b. Reversal of the gating polarity of gap junctions by negative charge substitutions in the N-terminus of connexin 32. *Biophys. J.* 79:2403–2415. http://dx.doi.org/10.1016/S0006-3495(00)76485-X

Reddy, A.S., and G.N. Sastry. 2005. Cation [M = H^+, Li^+, Na^+, K^+, Ca^{2+}, Mg^{2+}, NH_4^+, and NMe_4^+] interactions with the aromatic motifs of naturally occurring amino acids: a theoretical study. *J. Phys. Chem. A.* 109:8893–8903. http://dx.doi.org/10.1021/jp0525179

Ripps, H., H. Qian, and J. Zakevicius. 2004. Properties of connexin26 hemichannels expressed in *Xenopus* oocytes. *Cell. Mol. Neurobiol.* 24:647–665. http://dx.doi.org/10.1023/B:CEMN.0000036403.43484.3d

Rubinos, C., H.A. Sánchez, V.K. Verselis, and M. Srinivas. 2012. Mechanism of inhibition of connexin channels by the quinine derivative *N*-benzylquininium. *J. Gen. Physiol.* 139:69–82. http://dx.doi.org/10.1085/jgp.201110678

Sanchez, H.A., and V.K. Verselis. 2014. Aberrant Cx26 hemichannels and keratitis-ichthyosis-deafness syndrome: insights into syndromic hearing loss. *Front. Cell. Neurosci.* 8:354. http://dx.doi.org/10.3389/fncel.2014.00354

Sanchez, H.A., G. Mese, M. Srinivas, T.W. White, and V.K. Verselis. 2010. Differentially altered Ca^{2+} regulation and Ca^{2+} permeability in Cx26 hemichannels formed by the A40V and G45E mutations that cause keratitis ichthyosis deafness syndrome. *J. Gen. Physiol.* 136:47–62. http://dx.doi.org/10.1085/jgp.201010433

Sanchez, H.A., K. Villone, M. Srinivas, and V.K. Verselis. 2013. The D50N mutation and syndromic deafness: Altered Cx26 hemichannel properties caused by effects on the pore and intersubunit interactions. *J. Gen. Physiol.* 142:3–22. http://dx.doi.org/10.1085/jgp.201310962

Sanchez, H.A., R. Bienkowski, N. Slavi, M. Srinivas, and V.K. Verselis. 2014. Altered inhibition of Cx26 hemichannels by pH and Zn^{2+} in the A40V mutation associated with keratitis-ichthyosis-deafness syndrome. *J. Biol. Chem.* 289:21519–21532. http://dx.doi.org/10.1074/jbc.M114.578757

Smith, T.D., A. Mohankumar, P.J. Minogue, E.C. Beyer, V.M. Berthoud, and M. Koval. 2012. Cytoplasmic amino acids within the membrane interface region influence connexin oligomerization. *J. Membr. Biol.* 245:221–230. http://dx.doi.org/10.1007/s00232-012-9443-5

Srinivas, M., J. Kronengold, F.F. Bukauskas, T.A. Bargiello, and V.K. Verselis. 2005. Correlative studies of gating in Cx46 and Cx50 hemichannels and gap junction channels. *Biophys. J.* 88:1725–1739. http://dx.doi.org/10.1529/biophysj.104.054023

Downloaded from http://rupress.org/jgp/article-pdf/148/1/25/1795860/jgp_201611585.pdf by guest on 04 December 2025

Tang, Q., T.L. Dowd, V.K. Verselis, and T.A. Bargiello. 2009. Conformational changes in a pore-forming region underlie voltage-dependent "loop gating" of an unapposed connexin hemichannel. *J. Gen. Physiol.* 133:555–570. http://dx.doi.org/10.1085/jgp.200910207

Terrinoni, A., A. Codispoti, V. Serra, B. Didona, E. Bruno, R. Nisticò, M. Giustizieri, M. Alessandrini, E. Campione, and G. Melino. 2010. Connexin 26 (GJB2) mutations, causing KID Syndrome, are associated with cell death due to calcium gating deregulation. *Biochem. Biophys. Res. Commun.* 394:909–914. http://dx.doi.org/10.1016/j.bbrc.2010.03.073

Trexler, E.B., M.V. Bennett, T.A. Bargiello, and V.K. Verselis. 1996. Voltage gating and permeation in a gap junction hemichannel. *Proc. Natl. Acad. Sci. USA.* 93:5836–5841. http://dx.doi.org/10.1073/pnas.93.12.5836

Trexler, E.B., F.F. Bukauskas, M.V. Bennett, T.A. Bargiello, and V.K. Verselis. 1999. Rapid and direct effects of pH on connexins revealed by the connexin46 hemichannel preparation. *J. Gen. Physiol.* 113:721–742. http://dx.doi.org/10.1085/jgp.113.5.721

Trexler, E.B., F.F. Bukauskas, J. Kronengold, T.A. Bargiello, and V.K. Verselis. 2000. The first extracellular loop domain is a major determinant of charge selectivity in connexin46 channels. *Biophys. J.* 79:3036–3051. http://dx.doi.org/10.1016/S0006-3495(00)76539-8

van Steensel, M.A., P.M. Steijlen, R.S. Bladergroen, E.H. Hoefsloot, C.M. van Ravenswaaij-Arts, and M. van Geel. 2004. A phenotype resembling the Clouston syndrome with deafness is associated with a novel missense GJB2 mutation. *J. Invest. Dermatol.* 123:291–293. http://dx.doi.org/10.1111/j.0022-202X.2004.23204.x

Verselis, V.K. 2009. The connexin channel pore: pore-lining segments and residues. *In* Connexins: A Guide. A.L. Harris and D. Locke, editors. Humana Press, New York, NY. 77–102. http://dx.doi.org/10.1007/978-1-59745-489-6_3

Verselis, V.K., and M. Srinivas. 2008. Divalent cations regulate connexin hemichannels by modulating intrinsic voltage-dependent gating. *J. Gen. Physiol.* 132:315–327. http://dx.doi.org/10.1085/jgp.200810029

Verselis, V.K., C.S. Ginter, and T.A. Bargiello. 1994. Opposite voltage gating polarities of two closely related connexins. *Nature.* 368:348–351. http://dx.doi.org/10.1038/368348a0

Verselis, V.K., M.P. Trelles, C. Rubinos, T.A. Bargiello, and M. Srinivas. 2009. Loop gating of connexin hemichannels involves movement of pore-lining residues in the first extracellular loop domain. *J. Biol. Chem.* 284:4484–4493. http://dx.doi.org/10.1074/jbc.M807430200

Xu, J., and B.J. Nicholson. 2013. The role of connexins in ear and skin physiology — Functional insights from disease-associated mutations. *Biochim. Biophys. Acta.* 1828:167–178. http://dx.doi.org/10.1016/j.bbamem.2012.06.024

Zhou, X.W., A. Pfahnl, R. Werner, A. Hudder, A. Llanes, A. Luebke, and G. Dahl. 1997. Identification of a pore lining segment in gap junction hemichannels. *Biophys. J.* 72:1946–1953. http://dx.doi.org/10.1016/S0006-3495(97)78840-4

Downloaded from http://rupress.org/jgp/article-pdf/148/1/25/1795860/jgp_201611585.pdf by guest on 04 December 2025